Local structure of liquid GeTe via neutron scattering and *ab initio* simulations

J. Y. Raty,[1,2] V. V. Godlevsky,[3] J. P. Gaspard,[1] C. Bichara,[4] M. Bionducci,[5] R. Bellissent,[5] R. Céolin,[5] James R. Chelikowsky,[6] and Ph. Ghosez[1]

[1]*Département de Physique, B5, Université de Liège, B4000 Sart-Tilman, Belgique*

[2]*Lawrence Livermore National Laboratory, P.O. Box 808, Livermore, California 94550*

[3]*Department of Physics, Rutgers University, 136 Frelinghuysen Road, Piscataway, New Jersey 08854*

[4]*Centre de Recherche sur les Mécanismes de la Croissance Cristalline, CNRS, Campus de Luminy, Case 913, F13288 Marseille, Cedex 09, France*

[5]*Laboratoire Léon Brillouin, CEA-CNRS, F-91191, Gif-sur-Yvette cedex, France*

[6]*Department of Chemical Engineering and Materials Science, University of Minnesota, Minneapolis, Minnesota 55455*

(Received 24 January 2001; revised manuscript received 25 June 2001; published 19 February 2002)

We examine the local atomic order as well as some dynamic properties of the semiconducting liquid GeTe. We employ hot-neutron two-axis diffraction at three temperatures above the melting point and compare these results with *ab initio* molecular dynamics simulations. The simulations were based on interatomic forces derived from pseudopotentials constructed within density functional theory. At the melting temperature, the Peierls distortion responsible for the lower-temperature crystal phase is shown to manifest itself within the liquid structure. At higher temperatures in the liquid, increasing disorder in the Ge environment determines the eventual semiconductor-metal transition. The calculated kinematic viscosity of the liquid is found to agree with the experimental value and is shown to arise from the small diffusion coefficient of the Te atoms.

DOI: 10.1103/PhysRevB.65.115205 PACS number(s): 72.80.Ph, 61.12.−q, 71.15.Pd, 61.20.Ja

I. INTRODUCTION

The Ge_xTe_{1-x} semiconductor family exhibits many interesting properties, e.g., the ability to easily generate the amorphous phase and the possibility of thermally induced local crystallization.[1] Previous experiments have focused on the Te-rich compounds that are excellent glass-forming materials. Despite the importance of the glassy phase, the only studies examining the precursory liquid phase have been performed on the eutectic $Ge_{85}Te_{15}$ (Ref. 2) and $GeTe_2$ (Ref. 3) compounds. The local atomic structure of the liquids was not elucidated in these studies. Tsuchiya and Saitoh[4] found significant variations in the electrical conductivity, thermoelectric power, and specific volume in the melting phase just above the melting point. The most striking effects are measured for the eutectic composition and are accompanied by a semiconductor-metal transition.

These effects are present, to a lesser extent, in the *stoichiometric* GeTe compound. The dc conductivity of GeTe upon melting is only 9% higher than that of the solid ($2600\ \Omega^{-1}\,cm^{-1}$ versus $2400\ \Omega^{-1}\,cm^{-1}$), classifying GeTe as a semiconductor.[5] Upon further temperature increase, the dc conductivity of the melt increases very rapidly and reaches the values typical for metals.[6] However, this behavior is not accompanied by any anomalous variation of specific volume and thermal expansion coefficient as was observed for the eutectic composition.

The main physical aspects of the melting process of GeTe have been previously characterized by Glazov *et al.*[7] Yet the structure of the liquid and, especially, its relation with the semiconducting behavior of the melt remain unclear. In contrast to most tetrahedrally coordinated semiconductors (e.g., IV, III-V, and some II-VI), melting in GeTe is not associated with a semiconductor (SC)→metal (M) transition.[7] For compounds experiencing a SC→M transition upon melting, the sudden increase in dc conductivity is accompanied by a density increase, indicating a structural modification of the local atomic order in the liquid. For these semiconductors, neutron diffraction has demonstrated that the coordination number Z increases from the value of 4 in the crystal to a value ~ 6 in the melt.[8] Although this behavior is widely observed for IV and III-V compounds, some II-VI materials (HgSe, CdTe, and ZnTe) remain semiconducting in the melt. For the semiconducting liquids, both neutron diffraction[9] and, more recently, *ab initio* molecular dynamics simulations[10] have shown that an sp^3 covalent bonding configuration is preserved locally within the liquid structure.

GeTe presents an interesting case since it differs from all other studied IV, III-V, and II-VI semiconductors. At 900 °C ($T_m = 725$ °C) the coordination number of the liquid was measured to be 5.1,[11] noticeably larger than the value of ~ 4 common for semiconducting II-VI liquids (e.g., CdTe, ZnTe, HgSe), but clearly smaller than coordination number ~ 6 found for the metallic IV and III-VI liquids. A coordination of 5.1 is intermediate also for liquid chalcogenides (IV-VI materials), and it falls in between the coordination numbers of the lightest IV-VI liquid compounds (SnS and SnSe) and the heavier liquid SnTe.[11]

Two structural models have been proposed for the amorphous phase (a-GeTe), a more studied state of GeTe. The first model, assuming complete chemical disorder on the basis of x-ray and electron diffraction, extended x-ray absorption fine structure (EXAFS), Raman, infrared, and inverse photoemission spectroscopies, suggests the coordination to be 4 (for Ge atoms) and 2 (for Te atoms).[12] Another model, based on neutron diffraction and Mössbauer spectroscopy, supports a 3(Ge):3(Te) local order, closer to the crystalline one.[13] To date, there has been no evidence for chemical disorder in the amorphous or liquid phase. Neither of the two structural models support a structure of liquid GeTe (l-GeTe)

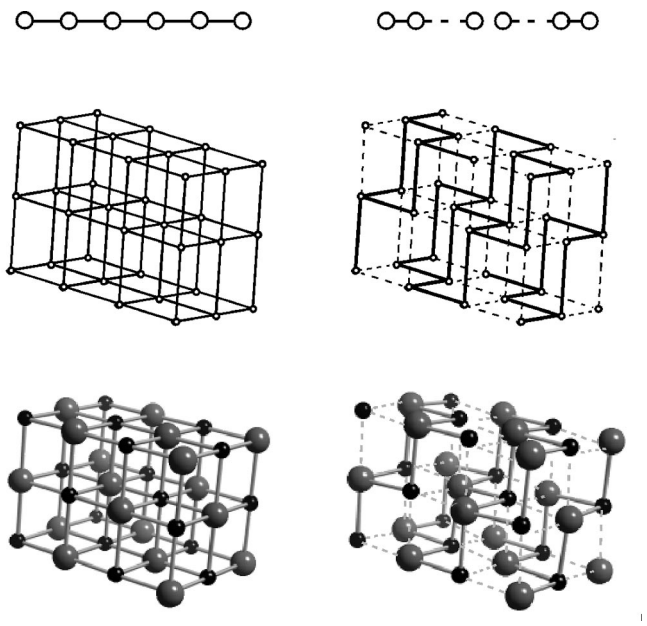

FIG. 1. Schematic view of the Peierls distortion. The undistorted structures are represented on the left and the Peierls distortion, on the right. Top: one-dimensional chain of half-filled *s* orbitals. Center: simple cubic structure with half-filled p orbitals (arsenic case). The shorter covalent bonds are represented by thick lines, the longer by dashed lines. Bottom: actual A7 and B1 structures of GeTe.

with 5.1 nearest neighbors. Such a structure has been interpreted as a sixfold-coordinated one with a certain concentration of vacancies in the first shell.[11] This kind of structure might explain the decrease in density (by 6.7%) observed upon melting. However, this explanation is not consistent with the definite SC behavior of *l*-GeTe, since a disordered sixfold-coordinated structure would involve a metallic type of conductivity with an appreciable jump in dc conductivity upon melting, as for group IV and III-V liquids.

The empirical rule of Joffe and Regel[14] is a practical criterion to determine the SC behavior of a liquid. It states that a crystalline semiconductor retains its semiconducting property in the liquid phase if the local atomic ordering is preserved upon melting. Although this rule may apply to describe the melting of SnS, SnSe, or GeS,[11] it clearly fails when considering GeTe. The change of the coordination number from 3 to ~ 5 suggests that there is an important modification in the local environment.

In its low-temperature crystalline phase (the α phase), GeTe (*c*-GeTe) assumes the $A7$ structure. The structure results from a Peierls distortion of a cubic $B1$ phase of *c*-GeTe. (The nature of the distortion depends on the filling ratio of valence orbitals and opens a gap at the Fermi level.[15]) The $A7$ structure can be imagined by starting with the $B1$ (NaCl-type) structure and then alternatively shortening and elongating bonds in the $\langle 100\rangle$, $\langle 010\rangle$, and $\langle 001\rangle$ directions with a slight modification of the bond angles (Fig. 1). In the $A7$ structure, the coordination number is 3. At the temperature of 430°C, *c*-GeTe undergoes a phase transition and the cubic $B1$ structure is recovered (β phase),[16,17] which has a coordination number of 6. The lattice and other structural parameters for the $A7$ and $B1$ crystal structures are given in Table I.

A fundamental understanding of the bonding mechanism of GeTe is crucial to explain the SC-SC type of melting and the rapid increase of σ as the temperature increases further, especially in the Te-rich part of the phase diagram.[4] Another possibility is that the local ordering in the liquid could be significantly different from that of the crystalline forms. A similar model has been proposed to explain the liquid state order in GeSe, which exhibits features similar to GeTe in both the solid and molten phases.[18,19] In both of these explanations of the *l*-GeTe microstructure, the evolution of *Z* combined with SC-type conductivity is inconsistant with the Joffe-Regel rule or with the hypothesis of perfect chemical ordering in the liquid. Also, the reasons for the gradual evolution of the liquid system to a metallic state remain unclear.

In our previous work,[20] we found evidence for a Peierls distortion using molecular dynamics. This distortion characterizes low-temperature *c*-GeTe, vanishes in the higher-temperature cubic $B1$ phase, and reappears in the liquid. As was demonstrated in Ref. 15, the concept of a Peierls distortion can be applied to a disordered structure provided that (i) there is a short-long alternation for the bond lengths (this alternation in two coordination shells is sufficient to open at least a pseudogap at the Fermi level), (ii) the bonding angle is close to 90°, and (iii) there is a ''sufficient'' chemical order (in the case of a binary alloy). So there is no need for an intermediate-range order or any longer periodicity to be able to apply the Peierls distortion concept, which in a liquid might as well be called a ''Jahn-Teller'' distortion. In Ref. 20, we showed that the *l*-GeTe structure verifies these three requirements.

In the present paper we describe in details the structure of *l*-GeTe, analyze the dynamics of the atomic motion, and explain the variations of the dc conductivity in the melt. In the first part of the paper, we present results of neutron diffraction experiments used to obtain additional data at 740° C and 800 °C and the first-principles technique used to simulate the liquid phase. We summarize the low- and high-temperature crystalline phases of GeTe in the second section. In the third section, we analyze the structure of the liquid and

TABLE I. Crystallographic parameters after Ref. 17. In the $A7$ phase, atoms are located in (u,u,u) and $-(u,u,u)$.

Phase	a (Å); α (deg); u	Z	r_1 (Å)	r_2 (Å)	Bond angle
α (20 °C)	$a=5.985$; 88.17°; 0.238	3+3	2.84	3.15	94.16°
β (432 °C)	$a=5.999$, 90°; 0.250	6	3.00	4.24	90°

discuss in detail the partial correlation functions and angular distributions. In the next section, we address the dynamics of the system via the diffusion coefficient and the self part of the Van Hove correlation function. Finally, we discuss the electrical properties of the simulated liquid.

II. TECHNIQUES

A. Experiment

We studied a Ge-Te (50:50) sample prepared by mixing pure elements in a silica tube (8 mm internal diameter and 1-mm-thick walls). The tube was sealed in vacuum with a minimized ''dead'' volume to avoid the change in composition upon melting due to the volatilization of the lightest element. Repeated heatings up to a temperature above the melting point have been performed to ensure a complete homogenization of the compound and to test the corrosion of the container. The corrosion was negligible, which allowed us to have a long experimental time at high temperature.

A neutron diffraction experiment was done on the two-axis 7C2 spectrometer in Leon Brillouin Laboratory (CEA-Saclay). The sample container was placed in a vanadium foil furnace, generating heat via the Joule effect. The whole cavity was maintained under high vacuum. Resistors were placed above and under the sample container to avoid uncontrolled convection and temperature fluctuations in the sample. We used 0.7035-Å-wavelength neutrons issued from the hot source of the reactor to reach the maximum transfer vector (q) of 15.9 Å^{-1}. This ensured minimal cutoff oscillations in the Fourier transform of the data. The data were recorded on a 640-cell detector and analyzed in a standard Paalman-Pings procedure.[21] After processing the spectra for the sample and furnace contributions, a correction for multiple scattering was performed using the Blech-Averbach coefficient.[22] Standard corrections have been applied to account for the inelastic and incoherent scattering.[23] The absolute normalization was checked by comparing the asymptotic scattering value at high angles with the one obtained with the scattering on a vanadium rod with the same diameter as the sample. Three data sets have been recorded for 12 h at 740, 800, and 900 °C.

B. Simulation

An ensemble of 64 atoms was used in a supercell geometry for our simulations. The size of the supercell was adjusted to the experimental liquid density ($\rho = 0.0335$ atoms/Å^3, $a = 12.4$ Å).[6] The interatomic forces were computed quantum mechanically using pseudopotentials within the density functional theory and the local density approximation (LDA). We employed a plane-wave basis for the expansion of the electronic wave functions[24] and we used Troullier-Martins peudopotentials[25] with Ceperley-Alder correlation.[26] We chose an energy cutoff equal to 9 Ry. To prepare the liquid ensemble, we performed Langevin dynamics.[24,27,28] Initially, we thermalized the liquid using a fictive heat bath and then removed the heat bath to examine the true dynamics. The time step used to integrate the equation of motion is taken as 300 a.u. (1 a.u. $= 2.4 \times 10^{-17}$ s). Starting from the $B1$ configuration, the liquid was thermalized at 6000 K during 3 ps. At this high ''fictive'' temperature, the memory of the initial condition was removed. After this randomization process, we gradually cooled the system down to the final temperature of 1000 K during a period of 3 ps. After 1.4 ps the liquid began to overheat and required rethermalization, which took 2 ps, before conducting the simulation during another 1.6 ps. The structural results we present in this paper are thus averaged over the configurations gathered during 3 ps at the final temperature, while the dynamical data are only averaged over the 1.6 ps uninterrupted simulation.

III. CRYSTALLINE GeTe: LOW- AND HIGH-TEMPERATURE PHASES

The phase diagram of Ge_xTe_{1-x} is quite rich.[16] In particular, there are three different crystalline phases: the low-temperature face-centered rhombohedral phase (α, $A7$) described above, the face-centered-cubic phase (β, $B1$) which appears around 432 °C with a volume contraction of $\sim 1\%$,[17] and finally an orthorhombic phase (γ) which is observed at low temperatures for $x_{Ge} > 50.5\%$.

Bonding has been extensively described in the α and β phases: The Baldereschi method gives a detailed description of the electronic charge densities.[29] In the rhombohedral phase, the structure can be attributed to almost pure $pp\sigma$ and $pp\pi$ bonds. On the other hand, a significant contribution from s states is observed in the cubic phase. A detailed study of the α-β transition has been done by first-principles calculations.[30] The band structure and pseudocharge densities support a simple tight-binding picture of the bonding as the s states are filled and bonding is ensured by $pp\sigma$ resonances: this favors the Peierls distortion mechanism.[15] This driving force for the Peierls distortion is somewhat counterbalanced by the ionic interaction, which stabilizes the cubic phase.[30]

With the same pseudopotentials used for the molecular dynamics simulations of l-GeTe, we calculated the total energy of the various crystalline phases. For the crystalline phase calculations, we used an energy cutoff of 15 Ry and sampled the Brillouin zone with 28 irreducible **k** points. In our calculations, the α phase is the stable one. The cell parameters of the α phase are reproduced within less than 1% accuracy ($a = 5.95$ Å, $\alpha = 89.09°$, $u = 0.2335$). Figure 2 shows that the configuration space around the energy minimum is very flat and elongated along compression of the a axis with fixed α (the distance u between Ge and Te atoms is relaxed for all values of a and α). This is related to the anisotropic compressibility of the layered structure. Compression perpendicular to the double atomic layers (along the $\langle 111 \rangle$ direction) is easier since interlayer bonding is mostly due to van der Waals interactions.

IV. STRUCTURE OF THE LIQUID

The total structure factor $S(q)$ of l-GeTe obtained by neutron diffraction is represented in Fig. 3. It is worth noting that $S(q)$ significantly differs from those of liquid GeSe and

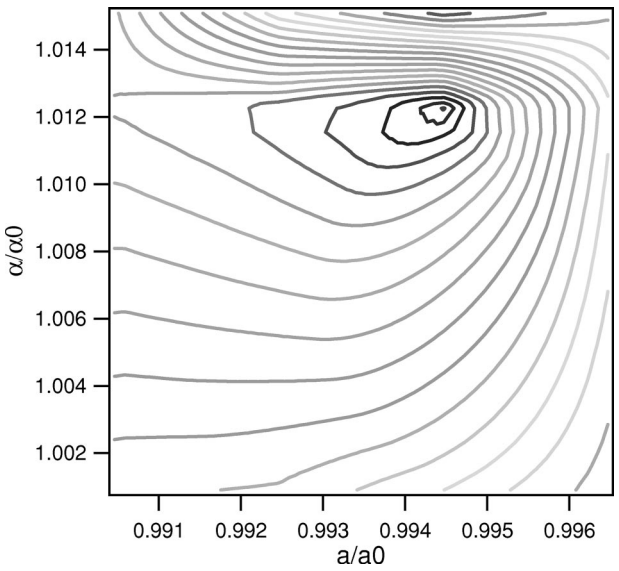

FIG. 2. Total energy as a function of the reduced cell parameters in rhombohedral notation. Contour lines are drawn with a spacing $\Delta E/E$ equal to $1\times10-6$.

GeS,[11,18,19] particularly in the region of the second peak $q \sim 3$ Å^{-1}, which is represented by a small shoulder in *l*-GeTe. This feature is well defined as a separate peak in both liquid GeSe and GeS. The disappearance of the second peak in *l*-GeTe cannot be attributed to the difference in coherent scattering cross sections σ, since σ(Te) is intermediate to σ(Se) and σ(S).[31] The peak disappearance must be related to the different structure of *l*-GeTe compared to *l*-GeSe and *l*-GeS. The difference is more pronounced as the temperature increases: the second peak is progressively

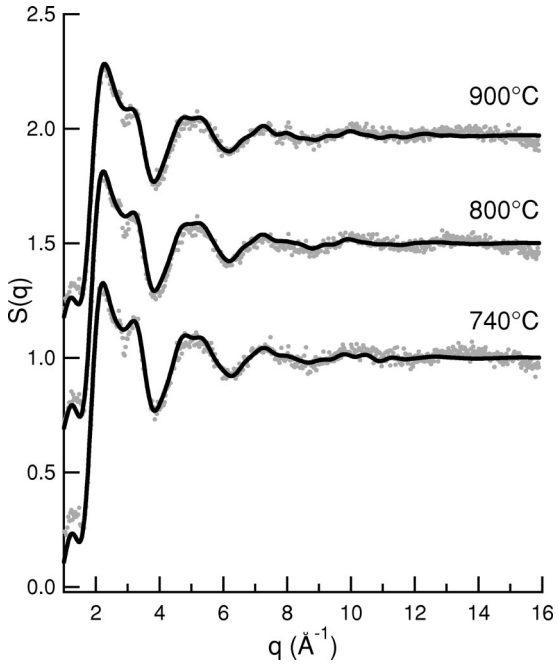

FIG. 3. Experimental $S(q)$ (dots). The lines are obtained by applying a high pass filter to the computed $g(r)$.

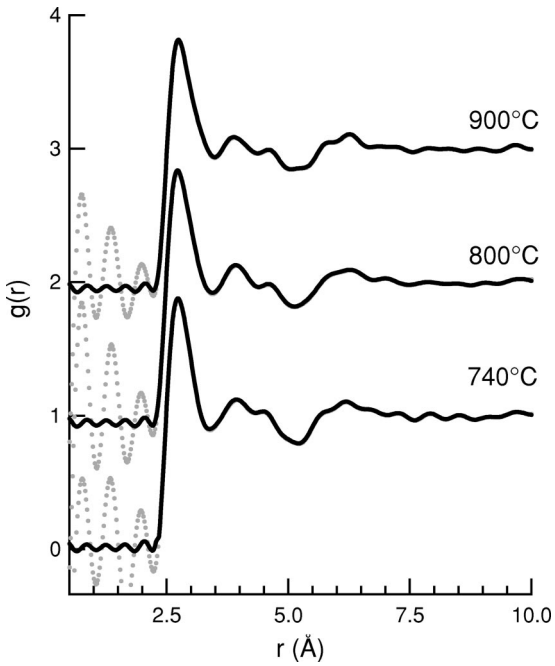

FIG. 4. Pair correlation functions $g(r)$ (dots). The lines are the $g(r)$ computed from the filtered $S(q)$.

smeared out of the spectrum. The pair correlation functions of *l*-GeTe obtained from the neutron scattering experiment are given on Fig. 4. The density ρ_0 was obtained from Ref. 6. The calculated $g(r)$ do not show any qualitative variation with temperature, but the quantitative evolution of the coordination number is not negligible as noted in Table II. *Z*, calculated by integrating $4\pi\rho_0 r^2 g(r)$ up to the first minimum ($r_c = 3.48$ Å), decreases significantly when lowering *T* to the melting point. The value of *Z* indicated in Table II is corrected from the difference in scattering lengths of Ge and Te assuming a complete chemical ordering:

$$Z_{corr} = \frac{Z_m}{4}\left(\frac{b_{Ge}}{b_{Te}} + \frac{b_{Te}}{b_{Ge}} + 2\right), \tag{1}$$

where b_i is the coherent scattering length of atom *i* and Z_m is the coordination number obtained by integration of $g(r)$.

As shown in Table II, the coordination number measured in the liquid phase is intermediate between those of the α phase ($Z=3$, layered structure) and of the β phase ($Z=6$, cubic structure). As the temperature approaches T_m from above, the coordination number of *l*-GeTe becomes closer to that of the α phase. It is interesting to note that in *l*-GeTe the

TABLE II. Distances, bonding angle, and coordination number in the crystalline and liquid phases.

GeTe	r_1 (Å)	r_2/r_1	Angle	Z_{corr}
20 °C (α)	2.843	1.107	94.16°	3
432 °C (β)	3.00	1.41 ($=\sqrt{2}$)	90°	6
740 °C (liq.)	2.72(2)	1.44(2)	92°(4)	3.90(50)
800 °C (liq.)	2.72(2)	1.44(2)	92°(4)	4.74(50)
900 °C (liq.)	2.74(2)	1.42(2)	91°(2)	5.03(50)

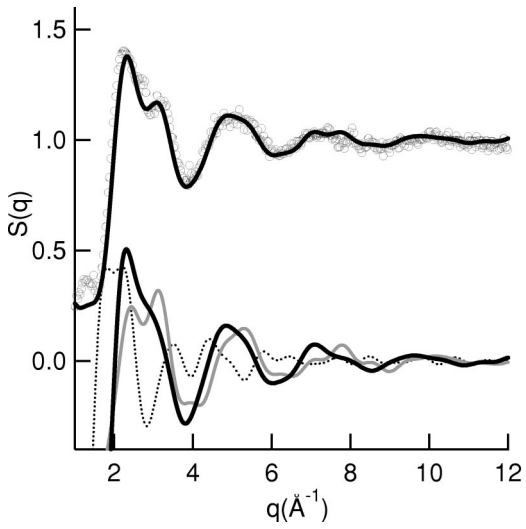

FIG. 5. Calculated structure factor $S(q)$ at 1000 K (plain line) compared with neutron diffraction $S(q)$ at 1173 K (symbols). Bottom: partial structure factors (shifted by -1) (S_{GeTe}, thick line; S_{GeGe}, gray line; S_{TeTe}, dots).

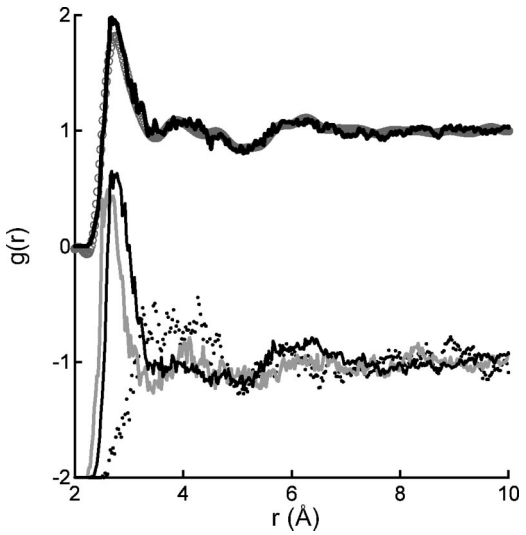

FIG. 6. Calculated total pair correlation function g(r) at 1000 K (plain line) compared with neutron diffraction $g(r)$ at 1173 K (symbols). Bottom: the partial $g(r)$ (g_{GeTe}, thick line; g_{GeGe}, gray line; g_{TeTe}, dots). The partials are shifted for clarity.

nearest-neighbor distance r_1 is lower by 4% to that in the α phase, while the estimated second-nearest-neighbor distance is larger than in α-GeTe.

These observations cannot be interpreted by invoking a vacancy model of the melt, i.e., an octohedral local environment with a surrounding concentration of vacancies (as was discussed previously). In such a model, the interatomic distance would not be larger than that of the crystal. However, a lowering of r_1 could be observed if the cubic local order of the β crystal distorts similarly to the α phase. The asymmetric shape of the first $g(r)$ peak suggests that the distances inside the first coordination shell are *not* equivalent. The larger volume of the liquid phase favors the Peierls distortion interpretation and, consequently, the creation of both shorter and longer bonds within the first shell.[15]

The partial structure factors of Fig. 5 were computed by Fourier transforming the partial pair correlation functions obtained from the molecular dynamics. We used the bound coherent scattering lengths of each element to obtain the total structure factor (in the Faber-Ziman definition[32]). The overall agreement with the 900 °C experiment is excellent, especially for the right shoulder of the first peak around 3 Å^{-1}. As we noticed before, the shoulder amplitude decreases when lowering T (see Fig. 3). Since the major partial contribution to the shoulder comes from the S_{GeTe} and S_{GeGe} partials (Fig. 5), we can predict it is mostly the Ge atomic environment that is modified for T closer to T_m.

The total $g(r)$ is accurately reproduced by the simulation. The total and partial $g(r)$'s are presented in Fig. 6. The total and partial coordination numbers of Table III indicate that the major contribution to the total $g(r)$ comes from Ge-Te bonds. There is a significant fraction of homopolar bonds contributed largely by Ge-Ge bonds. The total coordination of Ge atoms is larger than for Te atoms. It is clear from Fig. 6 that Te atoms repel each other outside the first coordination shell [$g_{Te\text{-}Te}(r)<1$, for $r<3.15$ Å]. As such, we believe the hypothetical tetrahedral order proposed recently[33] for the amorphous state to be inappropriate for the liquid, although the total coordination number is close to 4.

The atomic order inside the liquid is different from the crystalline phases of either the α or β structures. A similar observation, based on the partial $g(r)$ obtained by isotopic substitution and neutron diffraction, was recently made for liquid GeSe.[18,19] The heteropolar coordination number is important as it is very close to the value of 3 found in the Peierls-distorted structure of the α phase. This suggests that the structure of the semiconducting liquid, just above the melting point, might be closely related to the α phase.

The degree of chemical order may be measured by the Warren-Cowley parameter for liquids:[34]

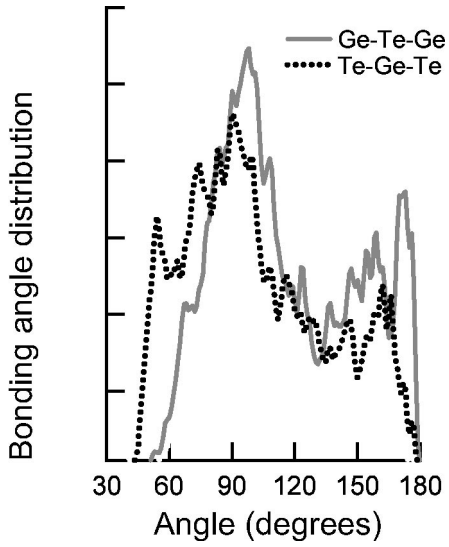

FIG. 7. Bond angle distributions, normalized by $\sin(\theta)$, in simulated liquid GeTe.

TABLE III. Total and partial coordination numbers in the crystalline and liquid phases. The first shell is defined by r_c.

	$Z_{Ge\text{-}Te}$	$Z_{Ge\text{-}Ge}$	$Z_{Te\text{-}Te}$	Z_{Ge}	Z_{Te}	Z_{Total}
20 °C (α)	3	0	0	3	3	3
432 °C (β)	6	0	0	6	6	6
740 °C (sim)	2.87(9)	2.56(9)	1.11(9)	5.43(19)	3.98(18)	4.70(19)

$$\alpha_x = \frac{1 - Z_{Te\text{-}Ge}/[c_{Te}c_{Ge}(Z_{Te}+Z_{Ge})]}{1 - Z_x/[c_{Te}c_{Ge}(Z_{Te}+Z_{Ge})]}, \qquad (2)$$

where $c_{Te}=c_{Ge}=0.5$ are the concentrations in Te and Ge, and the subscript x=Ge,Te. If $\alpha_x=1$, there is a perfect order (regular alternation of the atomic species). If $\alpha_x=0$, the structure is a random mixture. Another extreme case $\alpha_x=-1$ stands for a complete phase separation. In our simulations, $\alpha_{Ge}=0.17\pm0.02$ and $\alpha_{Te}=0.32\pm0.05$. It means that the local environment remains partially ordered especially around Te atoms.

We can also extract information on the liquid structure from the angular bonding distributions shown in Fig. 7. To construct the angular distributions, we calculated the angles between all possible triplets *A*-*B*-*C*. Atoms *A*, *B*, and *C* form the triplet *A*-*B*-*C* if *A* and *C* are in the first shell of reference atom *B* (or, in other words, if $|R_A-R_B|<r_c$ and $|R_B-R_C|<r_c$). The angle is defined as the angle between reference atom *B* and atoms *A* and *C*. The distributions were calculated using the same cutoff radius r_c for all types of bonds and normalized by the sine of the bonding angle θ, so that they would be flat in the case of the perfect gas. The heteropolar triplets angular distribution have pronounced maxima around 90° and 180°, with an additional minor peak around 60° present in Te-Ge-Te. The other distributions are almost featureless and flat between ~50° and 130°–150°.

Direct evidence for a Peierls distortion in the liquid is given by the angular limited triplet correlation (ALTC) function[35] plotted in Fig. 8. The ALCT function $g_{ang}(r_1,r_2)$ is a probability function normalized to that of an ideal gas (at the same density). The function corresponds to a probability of finding an atom *C* at a distance r_2 from an atom *B*, which is at a distance r_1 from the reference atom *A*. A constraint is placed on the position of atom *C*. Namely, the *BC* bond is contained in a cone of small angular aperture (here, 10°) around the *AB* axis. At high temperature (initial configuration thermalized at 6000 K), there is no correlation between the lengths of two successive bonds. At the final temperature of 1000 K, a correlation appears: a ''short'' bond of length r_1 is most probably followed, within the angular aperture of the cone, by a longer bond of length r_2 and vice versa. This is the structural signature of the Peierls distortion of the α phase. On the same plot, we also present ALTC function for a particular chemical order in the triplets. There is a strong correlation when the triplet has an alternating order (Ge-Te-Ge or Te-Ge-Te triplets), while there is almost negligible

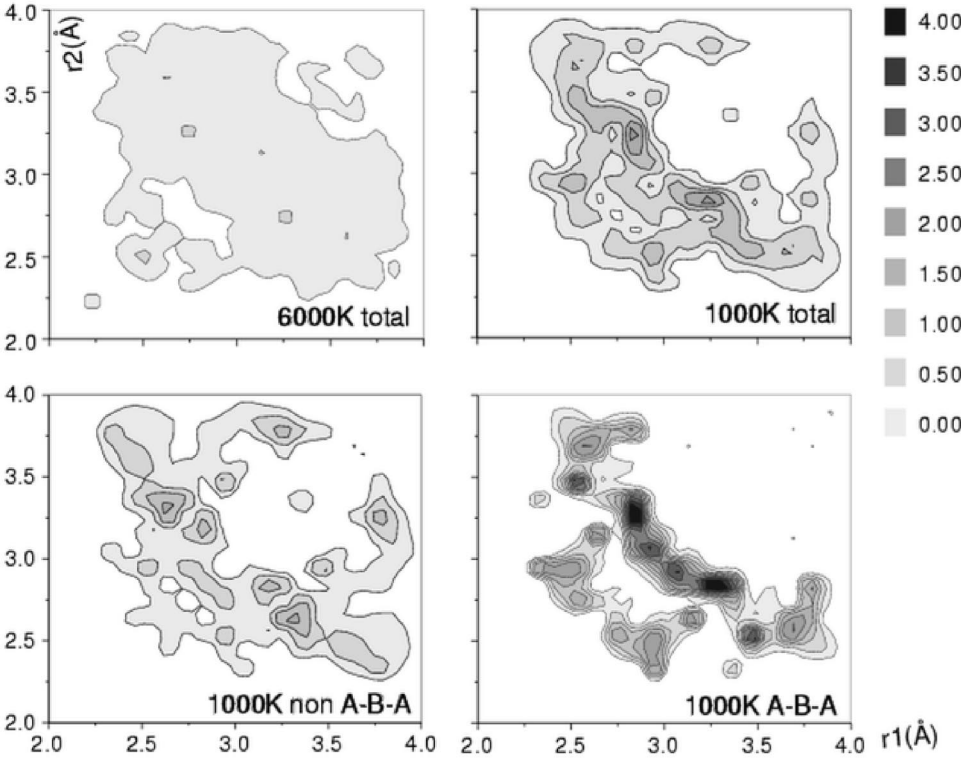

FIG. 8. Angular limited triplet correlation function $g_{ang}(r,r')$ (see text) for an angular aperture of 10°. The contour lines are obtained by averaging over 300 time steps (2.1 ps). Top of the figure: total $g_{ang}(r,r')$ at 6000 K (left) and 1000 K (right). Bottom of the figure: partial $g_{ang}(r,r')$ for non-alternating *A*-*A*-*A* and *A*-*A*-*B* triplets (left) and alternating *A*-*B*-*A* triplets (right).

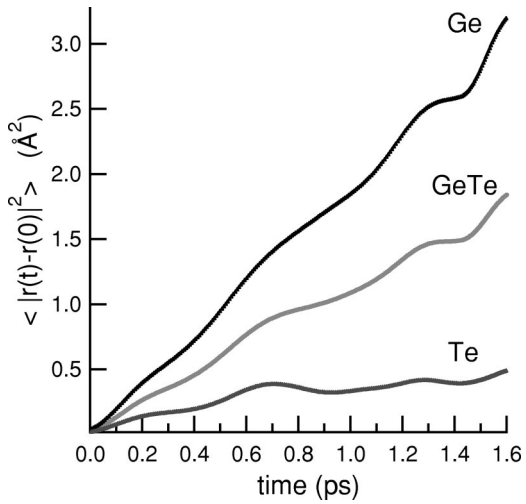

FIG. 9. Mean atomic squared displacement vs time in atomic units, for separate Ge and Te species and for all atoms (GeTe curve).

correlation for nonalternating triplets. The location of the correlation maximum ($r_1 \approx 2.8$ Å, $r_2 \approx 3.3$ Å) is quite similar to the first and second neighbors distances in the α phase (2.84 Å and 3.15 Å, respectively).

By comparing the high-temperature (6000 K) and low-temperature (1000 K) simulated liquids (Fig. 8), we see that the chemical ordering increases for T approaching T_m. This corresponds to more atoms having their local environment Peierls distorted: the coordination number should decrease towards the value of 3.9 (due to the presence of some Ge-Ge bonds) and the liquid electrical conductivity should decrease. This is in agreement with our neutron diffraction data as well as with the electrical measurements.[6]

V. DYNAMICAL ASPECTS

A direct way to quantify atomic dynamics comes from the diffusion coefficient, D. It can be directly extracted from the atomic displacement as a function of time:

$$D = \lim_{t\to\infty} \frac{\langle |\vec{r}_i(t) - \vec{r}_i(0)|^2 \rangle}{6t}, \tag{3}$$

where the brackets denote the average over all particles and $\vec{r}_i$ are the atomic positions. In Fig. 9, we plotted the squared atomic displacement as a function of time. For the partial atomic diffusivities, we obtain $D_{Ge} \sim 1.5 \times 10^{-5}$ cm^2 s^{-1} and $D_{Te} \sim 0.4 \times 10^{-5}$ cm^2 s^{-1}. The appreciable difference between the diffusivities (almost by a factor of 4) of Ge and Te cannot be accounted for simply by the mass difference. The fact that Ge has a higher mobility rather expresses the fact that a part of the Ge atoms move freely in the liquid, while the remaining Ge atoms bond with Te. These Te atoms can be imagined as attached to their three Ge neighbors and ''dragging'' them as they diffuse.

The shear viscosity is related to the diffusion coefficient of the liquid. In our case we use Stokes-Einstein formula[36] to obtain a rough estimate of the viscosity of a dense liquid:

$$\eta = \frac{k_B T}{6\pi r_0 D}, \tag{4}$$

where r_0 is the radius of an atomic sphere.[37] Using $r_0 = (\rho^{-1/3})$, with ρ the liquid density, we obtain a value of 2.54 cP, which is of the same order of magnitude as the experimental value $\sim$1.9 cP measured by Glazov and Shchelikov at 900 °C.[6]

However, the atomic displacements are not restricted to a simple Brownian motion. To quantify this deviation, we consider the self-part of the Van Hove function (autocorrelation function[38]) defined by

$$G_s(\vec{r},t) \simeq (1/N) \sum_{i=1}^{N} \langle \delta(\vec{r}_i(t) - \vec{r}_i(0) - \vec{r}) \rangle. \tag{5}$$

The average of $G_s(\vec{r},t)$ over all angles is the probability that an atom is found at time t at a distance r of its initial position. We plotted $f_s(r,t) = 4\pi r^2 G_s(r,t)$ for different values of time in Fig. 10. Each curve is obtained by averaging over 200 initial time steps and over all atoms of each kind. If the atoms follow a Brownian motion with the same diffusion coefficient, $f_s(r,t)$ should be Gaussian in the hydrodynamic limit[39] (dashed lines), with the peak broadening and shifting toward larger r with time.[40] We plotted in Fig. 10 (dotted lines) the model $f_s(r,t)$ built with the diffusion coefficient values obtained by Eq. (4):

$$f_s(r,t) \simeq \frac{r^2}{(4\pi)^{1/2}(Dt)^{3/2}} \exp\left(-\frac{r^2}{4Dt} \right). \tag{6}$$

In l-GeTe, the global evolution of $f_s(r,t)$ with time for Ge atoms is very close to the Brownian diffusion model. This is not true for Te atoms. The $f_s(r,t)$ first peak rapidly splits into two subpeaks with typical time larger than 0.5 ps. At 0.5 ps, these two peaks are located around $r = 0$ Å and $R_D = 0.5 - 0.6$ Å and a minimum appears around 0.4 Å while the hydrodynamic limit would give a maximum around 0.4 Å. This is a dynamical implication of the existence of the Peierls distortion in the liquid: R_D is comparable to the difference between the first and second neighbor shell radii in the liquid, $r_2 - r_1$. This backs up the interpretation of the local environment as a distorted octahedron, with a short bond ($r_1 \approx 2.8$ Å) facing a longer bond ($r_2 \approx 3.3$ Å) and the dynamical swapping between them. Another interpretation of this phenomenon is that there are two pseudoequilibrium positions of the center of the octahedron. This allows a simple ''floating octahedron'' model for the local order (see Fig. 11). The majority of Te atoms are centers of the distorted octahedra and have a significant rate of hopping to another pseudo equilibrium position inside the octahedron. The instantaneous configuration is almost the same as in the α crystal (with thermal broadening), with a dynamical switching of the bond lengths r_1 and r_2. This effect is not seen in the Van Hove self-correlation function of Ge atoms due to their high mobility and the numerous Ge-Ge bonds.

This model provides a summary of all the structural information obtained from the simulation: Te atoms have three

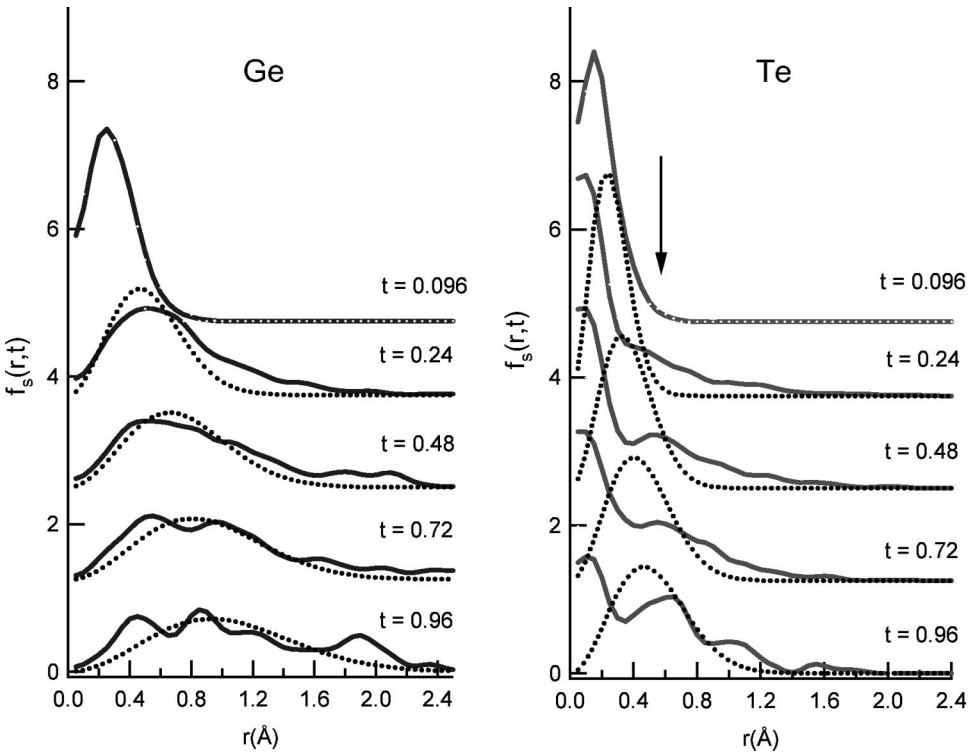

FIG. 10. Self part of the Van Hove correlation function $f_s(r,t_i)$, for $t_i=0.096-0.96$ ps (200 time steps). The $t_i=0.096$ curves are averaged over 400 initial time steps; the $t_i=0.96$ curves are averaged over 200 initial times. The dashed curves correspond to the hydrodynamic limit and are computed using formula (6).

first Ge neighbors at a distance $r1\approx 2.8$ Å (Tables II and III). In the directions of these three neighbors, there is a high probability to find the next atom at the distance $r2\approx 3.3$ Å (Fig. 8), and the Ge-Te-Ge bonding angle is peaked at 90° (Fig. 7). Finally, we see in Fig. 10 (right) that many of the Te atoms make ''jumps'' with an amplitude of ~ 0.5 Å on top of the diffusion and the time scale for this jump, or ''switching,'' is of the order of 0.5 ps.

VI. ELECTRICAL PROPERTIES

Experimentally, the electrical dc conductivity of *l*-GeTe (2600 $\Omega^{-1}\,\mathrm{cm}^{-1}$) does not change significantly from that of the crystal at the melting temperature (2400 $\Omega^{-1}\,\mathrm{cm}^{-1}$). As the temperature increases in the melt, the dc conductivity also increases; this represents a semiconducting behavior of the liquid.[8] The density of states (DOS) in *l*-GeTe was calculated in Ref. 20 where it was demonstrated that the Fermi level resides within a local minimum of the DOS. It also has been demonstrated[20] that the major bonding character of the levels in the vicinity of E_f corresponds to Te-*p*- and Ge-*p*-like orbitals. The angular distribution of the heteropolar triplets peaking at 90° (Fig. 7) also promotes the Peierls distortion.[15]

In our simulated liquid, we can determine the optical conductivity of the melt using the Kubo-Greenwood formula.[41] The conductivity is determined by the sum of all possible dipole transitions at a given frequency:

$$\sigma_r(\omega) = \frac{2\pi e^2}{3m^2\omega\Omega}\sum_{n,m}\sum_{\alpha=x,y,z}|\langle\psi_m|p_\alpha|\psi_n\rangle|^2\delta(E_n-E_m-\hbar\omega), \tag{7}$$

where E_i and ψ_i are the eigenvalues and eigenfunctions and Ω is the volume of the supercell.

Although our LDA calculations do not avoid the band gap problem,[42] the above expression appears to give a good estimate for the dc conductivity.[10] In addition, it provides a reasonable tool to distinguish between metallic and semiconducting characters of a liquid.[10] The extrapolation of $\sigma(\omega)$ to $\omega=0$ gives a value of the dc conductivity between 3000 and 4000 $\Omega^{-1}\,\mathrm{cm}^{-1}$ (Fig. 12). This agrees with the experimental value of 3100 $\Omega^{-1}\,\mathrm{cm}^{-1}$ measured at 900 °C.[6] Moreover, $\sigma(\omega)$ increases with ω to reach a maximum between 1.5 and 3 eV. This is the signature of a semiconducting liquid as $\sigma(\omega)$ would decrease from $\omega=0$ in the case of a metal.

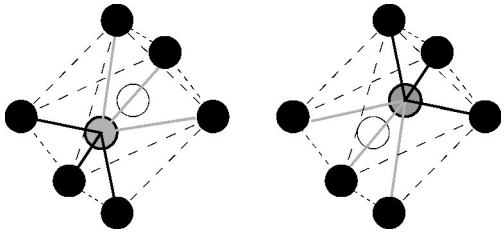

FIG. 11. Schematic view of the ''floating octahedron'' local order. The black and gray disks distinguish the two atom types. The center of a perfect octahedron is unstable vs two uncentered locations. The distances between these two locations is roughly given by RD (see text). The three shortest bonds are drawn in thick black lines and the three longest bonds are drawn in gray. The octahedron edges are represented by dashed lines.

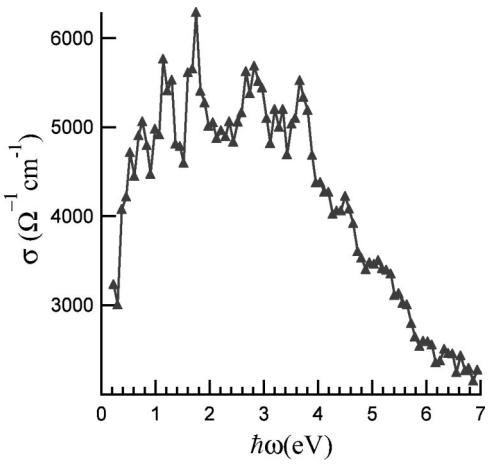

FIG. 12. Real part of the optical conductivity computed with formula (7) and averaged over ten instantaneous configurations.

VII. CONCLUSION

On the basis of neutron diffraction and molecular dynamics experiments, we have shown that the local order of liquid GeTe is partially Peierls distorted. The Peierls distortion, present in the low-temperature crystalline phase and absent in the high-temperature solid phase, is observed to reenter upon melting. Molecular dynamics simulations confirm the Peierls distortion on the basis of the following evidence in the melt: (i) structurally: the averaged local environment has alternation of short and long bonds along with the bond angles close to 90° characterizing the Peierls distortion; (ii) electronically: pronounced *p*-electron bonding and strong semiconductor character of $\sigma(w)$; (iii) dynamically: atoms of Te for which the Peierls distortion is more pronounced have a much smaller diffusion coefficient and a tendency to hop between the centers of a distorted octahedron. The reentrant Peierls distortion is directly dependent on the chemical order. At high temperatures, chemical ordering disappears as does the Peierls distortion. This appearance of the Peierls distortion is responsible for both the SC-M transition[6] and the decrease of the coordination number observed by neutron diffraction. Our study suggests that other IV-VI compounds such as GeSe could exhibit a similar behavior.

ACKNOWLEDGMENTS

This work was supported by the FNRS under Contract No. FRFC 9.4565.96F, the TMR-LSF program of the E.U., the NSF, NASA, and the Minnesota Supercomputing Institute. J.Y.R. is presently ''Chargé de Recherches du FNRS.''

[1] S.V. Phillips, R.E. Booth, and P.W. McMillan, J. Non-Cryst. Solids **4**, 510 (1970); A. Feltz, H.J. Buttner, F.J. Lippmann, and W. Maul, *ibid.* **8-10**, 64 (1972); S.R. Ovshinsky, Phys. Rev. Lett. **21**, 1450 (1968); J. Feinleib, J. de-Neufville, and S.C. Moss, Bull. Am. Phys. Soc. **15**, 245 (1970); C. Sie, P. Dugan, and S.C. Moss, J. Non-Cryst. Solids **8-10**, 377 (1972).

[2] E. Nicotera, M. Corchia, G. De Giorgi, F. Villa, and M. Antonini, J. Non-Cryst. Solids **11**, 417 (1973); H. Neumann, W. Hoyer, W. Matz, and M. Wobst, *ibid.* **97-98**, 1251 (1987); C. Bergman, C. Bichara, R. Bellissent, R. Céolin, J.P. Gaspard, and P. Chieux, An. Fis., Ser. B **86**, 138 (1990).

[3] K. Maruyama, M. Misawa, M. Inui, S. Takeda, Y. Kawakita, and S. Tamaki, J. Non-Cryst. Solids **205**, 106 (1996).

[4] Y. Tsuchiya and H. Saitoh, J. Phys. Soc. Jpn. **62**, 1272 (1993); Y. Tsuchiya, *ibid.* **60**, 227 (1991).

[5] J.E. Enderby, in *Amorphous and Liquid Semiconductors*, edited by J. Tauc (Plenum, New York, 1974), Chap. 7, p. 361.

[6] V.M. Glazov and O.D. Shchelikov, Sov. Phys. Semicond. **18**, 411 (1984).

[7] V.M. Glazov, S.N. Chizhevskaya, and N.N. Glagoleva, *Liquid Semiconductors* (Plenum, New York, 1969).

[8] J.E. Enderby and A.C. Barnes, Rep. Prog. Phys. **53**, 85 (1990), and references therein.

[9] J.-P. Gaspard, J.-Y. Raty, R. Céolin, and R. Bellissent, J. Non-Cryst. Solids **205-207**, 75 (1990).

[10] V.V. Godlevsky, J.J. Derby, and J.R. Chelikowsky, Phys. Rev. Lett. **81**, 4959 (1998).

[11] J.-Y. Raty, J.-P. Gaspard, M. Bionducci, R. Céolin, and R. Bellissent, J. Non-Cryst. Solids **250-252**, 277 (1999).

[12] S. Hosokawa, Y. Hari, T. Kouchi, I. Ono, M. Taniguchi, A. Hiraya, Y. Takata, N. Kosugi, and M. Watanabe, J. Phys.: Condens. Matter **10**, 1931 (1998); F. Betts, A. Bienenstock, and S.R. Ovshinsky, J. Non-Cryst. Solids **4**, 554 (1970); D.B. Dove, M.B. Heritage, K.L. Chopra, and S.K. Bahl, Appl. Phys. Lett. **16**, 138 (1970); O. Uemura, Y. Sagara, M. Tsushima, T. Kamikawa, and T. Satow, J. Non-Cryst. Solids **33**, 71 (1979); G.B. Fisher, J. Tauc, and Y. Verhelle, in *Amorphous and Liquid Semiconductors*, edited by J. Stuke (Taylor & Francis, London, 1974), p. 1259; Y. Maeda and M. Wakagi, Jpn. J. Appl. Phys., Part 1 **30**, 101 (1991).

[13] S.J. Pickart, Y.P. Sharma, and J.P. de Neufville, J. Non-Cryst. Solids **34**, 183 (1979); P. Boolchand, B.B. Triplett, S.S. Hanna, and J.P. de Neufville, *Mössbauer Effect Methodology* (Plenum, New York, 1974).

[14] A. Joffe and A. Regel, *Progress in Semiconductors* (Heywood, London, 1974), Vol. 4, p. 237.

[15] J.-P. Gaspard, A. Pellegatti, F. Marinelli, and C. Bichara, Philos. Mag. B **77**, 727 (1998).

[16] A. Schlieper, Y. Feutelais, S.G. Fries, B. Legendre, and R. Blachnik, CALPHAD: Comput. Coupling Phase Diagrams Thermochem. **23**, 1 (1999).

[17] T. Chattopadhyay, J.X. Boucherle, and H.G. von Schnering, Solid State Phys. **20**, 1431 (1987).

[18] P.S. Salmon and J. Liu, J. Phys.: Condens. Matter **6**, 1449 (1994).

[19] I. Petri, P.S. Salmon, and H.E. Fisher, J. Phys.: Condens. Matter **11**, 7051 (1999).

[20] J.Y. Raty, V. Godlevsky, P. Ghosez, C. Bichara, J.P. Gaspard, and J.R. Chelikowsky, Phys. Rev. Lett. **85**, 1950 (2000).

[21] H.H. Paalman and C.J. Pings, J. Appl. Phys. **33**, 2635 (1962).

[22] I.A. Blech and B.L. Averbach, Phys. Rev. **137**, A1113 (1965).

[23] G. Placzek, Phys. Rev. **86**, 377 (1952).
[24] R. N. Binggeli, J.L. Martins, and J.R. Chelikowsky, Phys. Rev. Lett. **68**, 2956 (1992).
[25] N. Troullier and J.L. Martins, Phys. Rev. B **43**, 1993 (1991).
[26] D.M. Ceperley and B.J. Alder, Phys. Rev. Lett. **45**, 566 (1980).
[27] R. Biswas and D. Hamann, Phys. Rev. B **34**, 895 (1986).
[28] J.R. Chelikowsky, N. Troullier, and N. Binggeli, Phys. Rev. B **49**, 114 (1994).
[29] H.M. Polatoglou, G. Theodorou, and N.A. Economou, J. Phys. C **16**, 817 (1983).
[30] K.M. Rabe and J.D. Joannopoulos, in *Electronic Phase Transitions*, edited by W. Hanke and Y.V. Kopaev (Elsevier, New York, 1992), p. 135.
[31] V.F. Sears, *Thermal Neutron Scattering Lengths and Cross Sections for Condensed Matter Research* (Atomic Energy of Canada Limited, Chalk River, 1984).
[32] T.E. Faber and J.M. Ziman, Philos. Mag. **11**, 153 (1965).
[33] S. Hosokawa, Y. Hari, T. Kouchi, I. Ono, M. Taniguchi, A. Hiraya, Y. Takata, N. Kosugi, and M. Watanabe, J. Phys.: Condens. Matter **10**, 1931 (1998).
[34] C. Wagner and H. Ruppersberg, At. Energy Rev. **1**, 101 (1981).
[35] C. Bichara, A. Pellegatti, and J.-P. Gaspard, Phys. Rev. B **47**, 5002 (1993).
[36] J. Frenkel, *Kinetic Theory of Liquids* (Oxford University Press, Oxford, 1946).
[37] J.P. Hansen and I.R. McDonald, *Theory of Simple Liquids* (Academic Press, London, 1976).
[38] L. van Hove, Phys. Rev. **95**, 249 (1954).
[39] J.N. Roux, J.L. Barrat, and J.P. Hansen, J. Phys.: Condens. Matter **1**, 7171 (1989).
[40] G. Wahnström, Phys. Rev. A **44**, 3752 (1991).
[41] R. Kubo, J. Phys. Soc. Jpn. **12**, 570 (1957); D. Greenwood, Proc. Phys. Soc. London **71**, 585 (1958).
[42] M.S. Hybertsen and S.G. Louie, Phys. Rev. B **35**, 5585 (1987); **35**, 5063 (1987); **37**, 2733 (1988); R.W. Godby, M. Schluter, and L.J. Sham, *ibid.* **35**, 4170 (1987); X. Blase, A. Rubio, S.G. Louie, and M.L. Cohen, *ibid.* **52**, R2225 (1995); H.N. Rojas, R.W. Godby, and R.J. Needs, Phys. Rev. Lett. **74**, 1827 (1995).